Communication

High Temperature Deformation Behavior of As-Cast Al-3Mg-0.25Sc Alloy

M. SURESH KUMAR, AMBRESHA, K. VENKATESWARLU, and V.R. RANGANATH

High temperature deformation behavior of as-cast Al-3Mg-0.25Sc alloy was characterized in a wide range of temperatures 573 K to 773 K (300 °C to 500 °C) and strain rates (0.001 to 10 s^{-1}). A threshold stress behavior is observed in the temperature range of 573 K to 673 K (300 °C to 400 °C) due to interaction of dislocations with precipitates. In the temperature range of 573 K to 623 K (300 °C to 350 °C), the dislocations are pinned by precipitates, following Orowan-bowing mechanism. At 673 K (400 °C), the dislocations bypass the particles by climb process. At high temperature and low strain rate of 723 K (450 °C), and 0.001 s^{-1}, respectively, the alloy exhibited high efficiency of power dissipation for optimal hot working process.

DOI: 10.1007/s11661-014-2276-3

Non-heat treatable Al-Mg alloys are employed in aerospace and other light material applications because of their superior weldability, formability, and corrosion resistance properties.[1,2] However, they exhibit relatively low strength values as compared to precipitation hardened Al-alloys.[3,4] The addition of minor quantities of Sc to Al-Mg alloys showed enhanced strength properties and was attributed to the formation of fine, stable, and coherent Al_3Sc precipitates.[5–7] There has been an extensive research on Al-Mg-Sc alloys, for example, on the effect of varying Mg and Sc contents for property enhancement,[8–11] precipitation kinetics,[12] dynamic recrystallization (DRX),[13–16] grain refinement by severe plastic deformation,[17–23] fatigue,[24,25] and high temperature properties (creep and superplasticity).[26,27] Fine-grained Al-Mg-Sc alloys are superplastic materials with reported tensile elongations in excess of 2000 pct at strain rates of ~1×10^{-2} s^{-1} in the temperature range 672 K to 823 K (399 °C to 550 °C).[28,29] In recent years, the hot deformation behavior of materials is modeled using processing maps that are developed based on dynamic materials model.[30] The principles and the basis for processing maps are discussed in detail elsewhere.[31] The efficiency of power dissipation resulting through the microstructural change during deformation, as a function of temperature and strain rate is represented by[32]

$$\eta = \frac{1}{2}\left[1 - \frac{1}{\sigma\dot{\varepsilon}}\left(\left(\frac{\sigma\dot{\varepsilon}}{m+1}\right)_{\dot{\varepsilon}=\dot{\varepsilon}_{\min}} + \int_{\dot{\varepsilon}_{\min}}^{\dot{\varepsilon}} \sigma \mathrm{d}\dot{\varepsilon}\right)\right]. \quad [1]$$

Moreover, the extremum principles of irreversible thermodynamics, as applied to continuum mechanics of large plastic flow, are used to develop a criterion for the onset of flow instability as[33]

$$\xi = \frac{2m}{\eta} - 1 < 0. \quad [2]$$

A super imposition of power dissipation map on the instability map constitutes a processing map, which reveals regimes of maximum power dissipation efficiency and the limiting conditions for the regimes of flow stability. Literature is limited on the processing maps and the deformation behavior of as-cast Al-3Mg-0.25Sc alloy. Therefore, the present investigation was undertaken with a specific objective of developing processing maps and to assess the rate controlling mechanisms for Al-3Mg-0.25Sc alloy with the help of hot deformation characteristics evaluated from flow behavior under compression at varying temperatures and strain rates.

Deformation mechanisms in aluminum and its alloys have been extensively studied.[34,35] For coarse-grained Al-Mg alloys deformed at elevated temperatures, two probable mechanisms could be considered. The first mechanism might be the power law dislocation creep with an average n value of ~ 5 with no dependence on grain size,[36] represented as:

$$\dot{\varepsilon} = B(Eb/kT)D_{\text{eff}}\left(\frac{\sigma - \sigma_{\text{th}}}{E}\right),$$

where B is coefficient related to dislocation creep, E is Young's modulus, b is the magnitude of Burger vector, k the Boltzmann's constant, D_{eff} is the effective diffusion coefficient, σ is the applied stress, and σ_{th} is the threshold stress. For Al-alloys with high content of Mg, the second mechanism could be the solute drag creep. The rate controlling equation for this mechanism is[37]

$$\varepsilon = C(kT/E)D_S\left(\frac{\sigma}{E}\right)^3,$$

where C is a constant and D_s is the diffusion coefficient of the solute in the Al matrix.

The material chosen for the present study is as-cast Al-3Mg-0.25Sc alloy. Required quantity of Al-2Sc master alloy was added to Al-3Mg melt to yield Al-3Mg-0.25Sc. Care was taken to remove the gases present in the melt by addition of ~1 pct hexa-chloroethane. The melt was poured into graphite molds to prepare rods of

M. SURESH KUMAR, Scientist, AMBRESHA, Project Assistant, and K. VENKATESWARLU, Principal Scientist, are with the Materials Science Division, CSIR-National Aerospace Laboratories, Kodihalli, Bangalore 560017, India. Contact e-mail: karodi2002@yahoo.co.in V.R. RANGANATH, Chief Scientist, is with the Structures Division, CSIR-National Aerospace Laboratories, Kodihalli, Bangalore 560017, India.
Manuscript submitted March 19, 2013.

Journal : MMTA_11661 Dispatch : 25-3-2014 Pages : 5
MS Code : 2276 ☐ LE ☐ CP ☐ TYPESET ☐ DISK

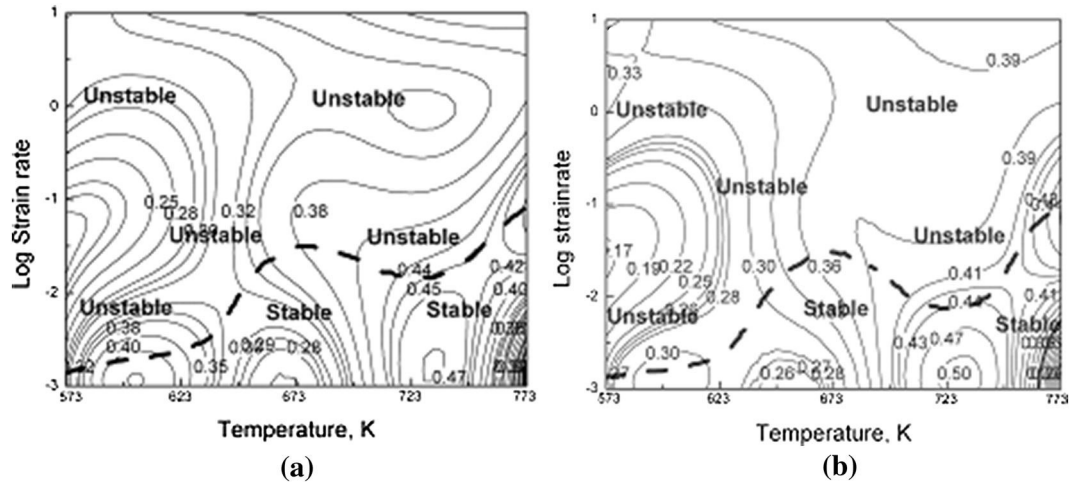

Fig. 3—Processing map of Al-3Mg-0.2Sc alloy for deformation up to a true plastic strain of (*a*) 0.4 and (*b*) 0.7.

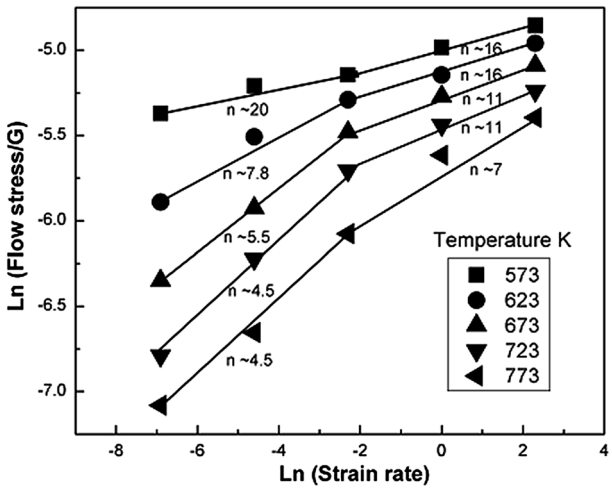

Fig. 4—Apparent stress exponent values for different temperatures and strain rates.

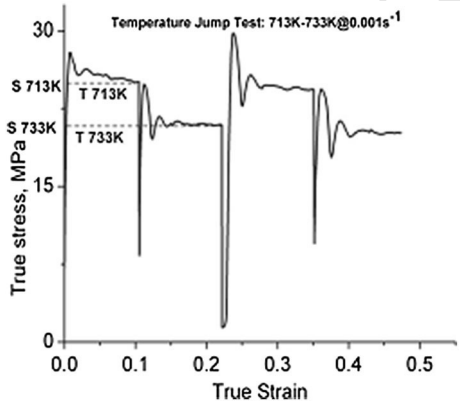

Fig. 5—True stress *vs* True strain behavior during temperature jump tests at constant strain rate of 0.001 s^{-1} for the alloy deformed at 723 K (450 °C).

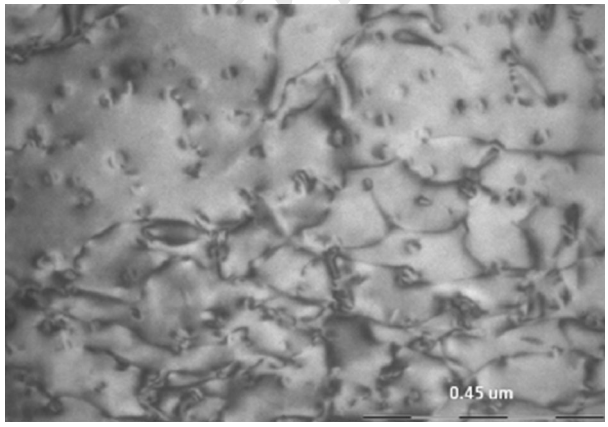

Fig. 6—TEM image of the alloy deformed at 573 K (300 °C) at 0.001 s^{-1}.

precipitate shearing mechanism was calculated as per Reference 43. The rise in yield stress due to order strengthening ($\Delta\sigma_{os}$), coherency strengthening ($\Delta\sigma_{cs}$), and modulus mismatch strengthening ($\Delta\sigma_{ms}$) was 166, 100, and 237 MPa, respectively. The larger of the $\Delta\sigma_{os}$ or ($\Delta\sigma_{cs} + \Delta\sigma_{ms}$) is the total strength increment from shearing mechanism. This mechanism could be excluded since it would lead to an increase in yield stress values by a factor of 2.2 to 5. The increase in yield stress due to Orowan mechanism ($\Delta\sigma_{or}$) is 50 MPa and that is in close agreement with the observed threshold value (~75 MPa). An Orowan mechanism therefore is most likely operating mechanism at 573 K (300 °C). However, at 673 K (400 °C), the derived threshold stress value is 4 MPa which is significantly lower than the value obtained following either Orowan mechanism or precipitate shearing mechanism and, as such, cannot be the operating mechanism. Therefore, at 673 K (400 °C), dislocations appear to bypass coherent particles by climb. In climb-controlled bypass, widely accepted mechanism is general-climb, in which, dislocations experience a small increase in length while climbing over the precipitates leading to smaller threshold stress values of the order of 0.02 ($\Delta\sigma_{or}$). This value agrees well with the threshold stress (~4 MPa) obtained at 673 K (400 °C). Hence, it is suggested that climb mechanism is

Journal : MMTA_11661 Dispatch : 25-3-2014 Pages : 5
MS Code : 2276 LE CP TYPESET DISK

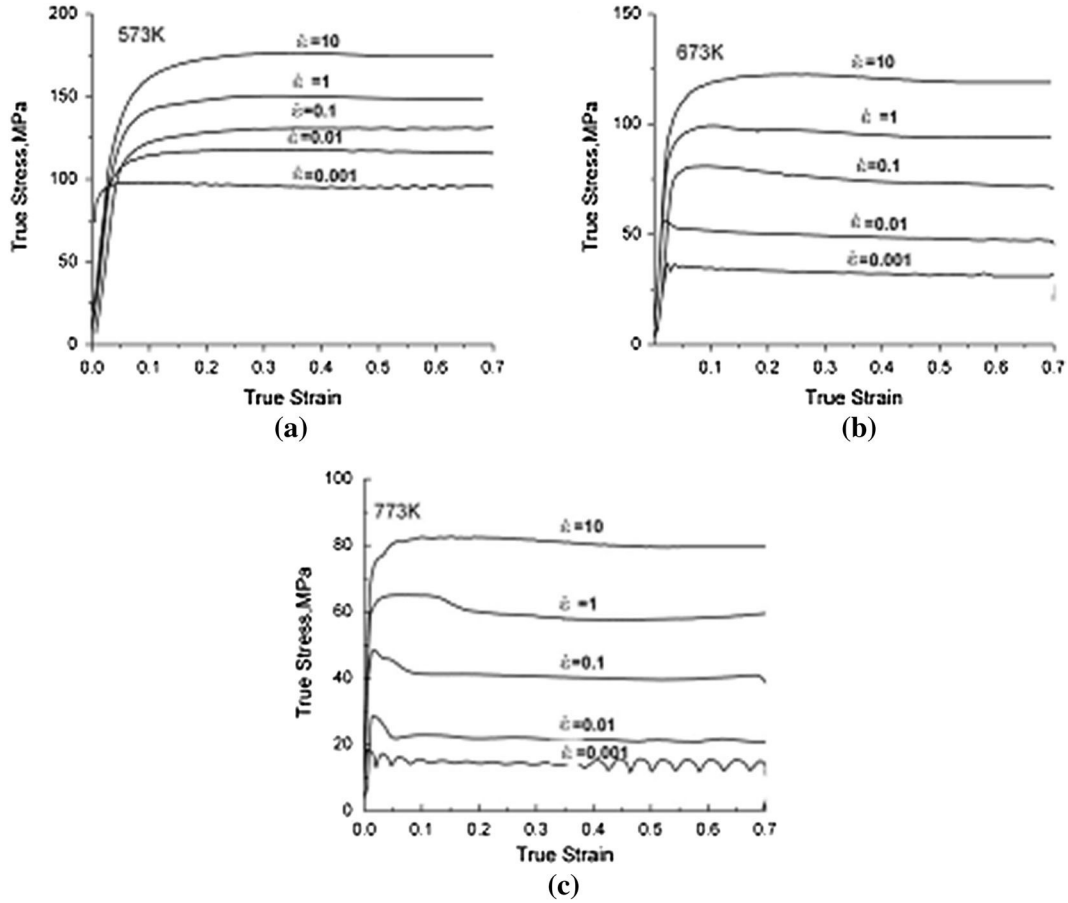

Fig. 1—Effect of strain rate on the deformation behavior of Al-3Mg-0.2Sc at various temperatures: (*a*) 573 K (300 °C); (*b*) 673 K (400 °C); (*c*) 773 K (500 °C).

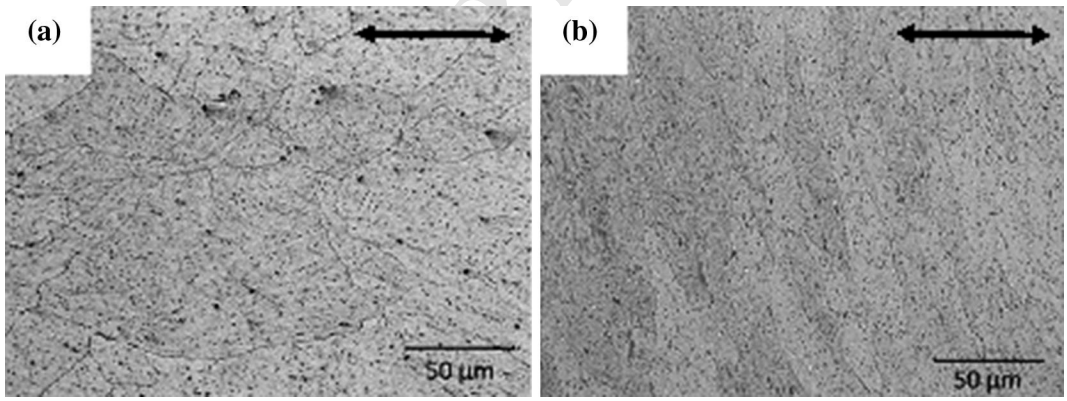

Fig. 2—Optical microstructures of the alloy deformed at (*a*) 773 K (500 °C) and $\dot{\varepsilon} = 0.001\ s^{-1}$; (*b*) 573 K (300 °C) and $\dot{\varepsilon} = 0.001\ s^{-1}$. Arrows indicate loading direction.

to Mg diffusion in Al matrix (136 kJ mol^{-1}) and self-diffusion of pure Al (142 kJ mol^{-1}). The microstructure of the samples tested at 573 K (300 °C) at strain rate of 0.001 s^{-1} shows fine coherent Al_3Sc precipitates having mean radii of 15 nm. The micrographs were processed using ImageJ, a public domain image processing software, to analyze the size of the particles. It may be observed from Figure 6 that multiple dislocations are interacting with precipitate particles. The coherent phase inhibits dislocation motion necessary to form subgrains or a recrystallized structure. The threshold stresses in precipitate (coherent) strengthened alloys at high temperature may result due to various possible mechanisms *viz*., precipitate shearing, Orowan bowing, dislocation climb over precipitates. The increase in yield stress at 573 K (300 °C) due to Orowan mechanism and

Journal : MMTA_11661 Dispatch : 25-3-2014 Pages : 5
MS Code : 2276 ☐ LE ☐ CP ☐ TYPESET ☐ DISK

diameter 12.0 and 80 mm length and these rods were machined to 10 mm diameter and 13 mm height. All the specimens were homogenized at 723 K (450 °C) for 1 hour. The specimens were deformed in compression by using a computer-controlled servo-hydraulic machine in the temperature range of 573 K to 773 K (300 °C to 500 °C) at intervals of 323 K (50 °C) and at constant true strain rates ranging from 0.001 to 10 s^{-1}. All specimens were deformed to a true strain of 0.7 followed by immediate water quenching to preserve the as-deformed microstructure. The flow stress data obtained at different temperatures, strain rates, and strains were corrected for adiabatic temperature as suggested by Goetz and Semiatin.[38] The values of strain rate sensitivity (m) were computed for each sample, at different temperatures, from the local values of slopes of the logarithmic plots between stress and strain rate. The efficiency of power dissipation and instability parameter were calculated using Eqs. [1] and [2]. Routine microstructural examination was conducted with the aid of optical microscope and Transmission Electron Microscope (TEM). A few selected samples were sectioned, polished and etched with Keller's reagent before microstructure, both, in longitudinal and in tangential directions was studied.

Flow Behavior Figure 1 shows the flow behavior of the alloy at representative temperatures of 573 K, 673 K, and 773 K (300 °C, 400 °C, and 500 °C) for different strain rates. Three aspects can be clearly seen from the deformation response of the present alloy. First, at any given temperature, strain rate has a significant effect on flow stress, the flow stress increases with increasing strain rate (positive strain rate sensitivity). Second, the flow stress decreases with increasing test temperature. Third, the shape of the flow curve changes with decreasing strain rate increasingly prominent at high temperatures. It may be observed from the plots that a steady state flow sets in at low temperature *i.e.*, 573 K (300 °C), at all strain rates in the entire strain range without showing any single peak stress. At a temperature of 773 K (500 °C), however, irrespective of the strain rate, all the curves show a peak stress followed by either a steady state behavior or oscillating nature. It has been reported that DRX could be the operating mechanism when the flow curves exhibit single peak or multiple oscillations.[39] Microstructures of the sample tested at a temperature of 773 K (500 °C) and 0.001 s^{-1} strain rate shows equiaxed grains (Figure 2(a)) typical of DRX microstructure. On the other hand, the sample tested at temperature of 573 K (300 °C) and strain rate of 0.001 s^{-1} strain rate shows elongated grains in both longitudinal and tangential sections (Figure 2(b)). The minor oscillations observed in the flow curves of samples tested at 573 K and 673 K (300 °C and 400 °C) could possibly be due to dynamic strain aging phenomenon.[13]

Processing Maps Figures 3(a) and (b) are processing maps developed for the Al-Mg-Sc alloy deformed to a true strain of 0.4 and 0.7, respectively. The numbers accompanying each contour represent efficiency of power dissipation and a dotted line delineates the region of instability. The processing maps appear to be independent of strain with little or no change. Processing maps display highest power dissipation at 723 K (450 °C) at a strain rate of 0.001 s^{-1}, with a peak efficiency of ~50 pct. At lower temperature range 573 K to 623 K, (300 °C to 350 °C), the region of instability appears for quite a wider strain rate range starting from 0.001 to 10 s^{-1}. However, at higher temperature [>723 K (>450 °C)] the instability region appears only from a strain rate range of 0.1 to 10 s^{-1}.

Deformation Mechanisms The apparent stress exponent, n_a, (Figure 4) was determined from the *ln* (flow stress/G) *vs ln* (strain rate) plots and found to be 4.5 at temperatures of 723 K and 773 K (450 °C and 500 °C) in the strain rate range from 0.001 to 0.1 s^{-1}. At other temperatures *i.e.,* 573 K, 623 K, and 673 K (300 °C, 350 °C, and 400 °C), n_a was determined to be 20, 7.8, and 5.5, respectively. The apparent activation energy, Q_a, calculated from temperature jump test data at a constant strain rate of 0.001 s^{-1} for 723 K and 773 K (450 °C and 500 °C) temperatures is 136 and 146 kJ mol^{-1}, respectively. A typical temperature jump test data for 723 K (450 °C) is shown in Figure 5. The apparent activation energy (Q_a) values at a constant strain rate of 0.001 s^{-1} for 573 K, 623 K, and 673 K (300 °C, 350 °C, and 400 °C) temperatures are 650, 246, and 175 kJ mol^{-1}, respectively. At these temperatures, it appears that a threshold stress, σ_{th}, exists below which the deformation rate is negligible.[40] The value of σ_{th} was determined using a linear extrapolation on a double-linear plot of $(\dot{\varepsilon})^{1/n}$ *vs* σ, for n values of 2, 3, 4, 5, 6, and 7 at each temperature. The most probable true stress exponent n_t, appears to be 5.0, which corresponded to higher correlation coefficients. The intercept of fitted straight line on stress axis at zero strain rate gives the value of σ_{th}. In general, a very low strain rate (creep) data is required for calculation of threshold stress. However, literature shows that data available for strain rates ranging between 0.0001 and 0.01 s^{-1} can be employed to calculate σ_{th} and the same is followed in this study.[41] The obtained σ_{th} for 573 K, 623 K, and 673 K (300 °C, 350 °C, and 400 °C) were 75, 30, and 4 MPa respectively. The threshold stress is appreciably high at low deformation temperatures and decreases gradually with increasing temperature. A relationship between n_a and n_t proposed by Park and Mohamed[42] was used to substantiate the results. The relationship is represented as:

$$n_a/n_t = \sigma/(\sigma - \sigma_{th}).$$

In the present study, for instance, the effective stress after considering threshold stress, was determined to be 22 MPa at temperature of 573 K (300 °C) and strain rate of 0.001 s^{-1}. Therefore, the value of $\sigma/(\sigma - \sigma_{th})$ is ~4.3, whose value is close to the ratio of n_a and n_t. Estimated value of true stress exponent thus appears reasonable. If the threshold value is taken into consideration, the true activation energy (Q_t) values at constant strain rate of 0.001 s^{-1} for 573 K, 623 K, and 673 K (300 °C, 350 °C, and 400 °C) temperatures are similar, at ~135 kJ mol^{-1}, the value is identical as that determined for temperature range of 723 K to 773 K (450 °C to 500 °C). The activation energy value is close

Journal : MMTA_11661 Dispatch : 25-3-2014 Pages : 5
MS Code : 2276 ☐ LE ☐ CP ☐ TYPESET ☐ DISK

operative at a temperature of 673 K (400 °C) and strain rate of 0.001 s^{-1}.

Processing maps were developed for the as-cast Al-3Mg-0.25Sc alloy from compression test data in the temperature range of 573 K to 773 K (300 °C to 500 °C) and strain rate range of 0.001 to 10 s^{-1}. The maps showed safe hot working regime with highest efficiency of power dissipation at a temperature of 723 K (450 °C) and strain rate of 0.001 s^{-1}. Study of thermal activation parameters revealed a transition in the rate control mechanism from Orowan bowing at lower temperature *i.e.*, 573 K (300 °C) to dislocation climb bypass over particles at higher temperatures *i.e.*, 673 K (400 °C).

The authors would like to thank Dr. S.K. Bhaumik and Mr. N. Jaganathan CSIR-NAL, Bangalore for a fruitful discussion, and for assisting in the test program, respectively.

REFERENCES

1. ASM Metals Handbook: *Properties and Selection: Non-ferrous Alloys and Special-Purpose Materials*, 10th ed., ASM International, Materials Park, OH, 1990, vol. 2, pp. 490–91.
2. I.J. Polmear: *Light Alloys Metallurgy of the Light Metals*, 3rd ed., Arnold Publishers, London, 1995, pp. 185–86.
3. L.S. Toropova, D.G. Eskin, M.L. Kharakterova, and T.V. Dobatkina: *Advanced Aluminum Alloys Containing Scandium*, Gordon and Breach, Amsterdam, 1998, pp. 133–60.
4. V.G. Davydov, T.D. Rostova, V.V. Zakharov, Yu.A. Filatove, and V.I. Yelagin: *Mater. Sci. Eng.*, 2000, vol. 30A, pp. 280–97.
5. M.D. Drits, L.S. Toropova, and Yu.G. Bykov: *Metalloved. Term. Obbrab. Met.*, 1983, vol. 7, pp. 60–63.
6. N. Blake and M.A. Hopkins: *J. Mater. Sci.*, 1985, vol. 20, pp. 2861–67.
7. T.V.I. Wirtz, G. Lütejering, A. Gysler, B. Lenczowski, and R. Rauh: *Mater. Sci. Forum*, 2000, vol. 1489, pp. 331–37.
8. L.I. Kaygorodova and V.P. Domashnikov: *Phys. Met. Metall.*, 1990, vol. 68, pp. 160–64.
9. Yu.M. Vainblat, S.S. Khayurov, and L.B. Ber: *Tekhnol Legk Spl.*, 1996, vol. 3, pp. 18–22.
10. L.M. Dougherty, I.M. Robertson, and J.S. Vetrano: *Acta Mater.*, 2003, vol. 51, pp. 4367–78.
11. T. Aiura, N. Sugawara, and Y. Miura: *Mater. Sci. Eng.*, 2000, vol. 280, pp. 139–45.
12. R. Roumina and C.W. Sinclair: *Acta Mater.*, 2010, vol. 58, pp. 111–21.
13. K. Ihara and Y. Miura: *Mater. Sci. Eng. A*, 2004, vol. 387, pp. 647–50.
14. Y.W. Riddle and T.H. Sanders: *Metall. Mater. Trans. A*, 2004, vol. 35A, pp. 341–50.
15. V. Ocenasek and M. Slamova: *Mater. Charact.*, 2001, vol. 47 (2), pp. 157–62.
16. H.G. Paris, T.H. Sanders Jr, and Y.W. Riddle: *Proc. ICAA-6*, 1998, pp. 449–504.
17. T.G. Nieh, R. Kaibyshev, L.M. Hsiung, N. Nguyen, and J. Wadsworth: *Scripta Mater.*, 1997, vol. 36, pp. 1011–16.
18. P.B. Berbon, S. Komura, A. Utsunomiya, Z. Horita, M. Furukawa, M. Nemoto, and T.G. Langdon: *Mater. Trans. JIM*, 1999, vol. 40, pp. 772–78.
19. M. Furukawa, A. Utsunomiya, K. Matsubara, Z. Horita, and T.G. Langdon: *Acta Mater.*, 2001, vol. 49, pp. 3829–38.
20. T.G. Nieh, L.M. Hsiung, J. Wadsworth, and R. Kaibyshev: *Acta Mater.*, 1998, vol. 46, pp. 2789–2800.
21. Z. Horita, M. Furukawa, M. Nemoto, A.J. Barnes, and T.G. Langdon: *Acta Mater.*, 2000, vol. 48, pp. 3633–40.
22. S. Komura, Z. Horita, M. Furukawa, M. Nemoto, and T.G. Langdon: *Metall. Mater. Trans. A*, 2001, vol. 32A, pp. 707–16.
23. N. Balasubramanian and T.G. Langdon: *Mater. Sci. Eng. A*, 2005, vol. 410, pp. 476–79.
24. O. Roder, T. Wirtz, V. Gysler, and G. Lütejering: *Mater. Sci. Eng. A*, 1997, vol. 181, pp. 234–36.
25. C. Watanabe, C.Y. Jin, R. Monzen, and K. Kitagawa: *Int. J. Fatigue*, 2008, vol. 30, pp. 635–41.
26. M. Kamachi, M. Furukawa, Z. Horita, and T.G. Langdon: *Mater. Trans.*, 2004, vol. 45, pp. 2521–24.
27. F. Musin, R. Kaibyshev, Y. Motohashi, and G. Itoh: *Scripta Mater.*, 2004, vol. 50, pp. 511–16.
28. R.R. Sawtell and C.L. Jensen: *Metall. Trans. A*, 1990, vol. 21A, pp. 421–30.
29. T.G. Neih, L.M. Hsiung, J. Wadsworth, and R. Kaibyshev: *Acta Metall.*, 1998, vol. 46, pp. 2789–2800.
30. Y.V.R.K. Prasad: *Ind. J. Technol.*, 1990, vol. 28, pp. 435–51.
31. Y.V.R.K. Prasad, H.L. Gegel, S.M. Doraivelu, J.C. Malas, J.T. Morgan, L.A. Lark, and D.R. Barker: *Metall. Trans. A*, 1984, vol. 15A, pp. 883–88.
32. H. Ziegler: *Progress in Solid Mechanics*, Wiley, New York, NY, 1963, vol. 4, pp. 93–95.
33. S.V.S. Narayana Murty and B. Nageswara Rao: *Mater. Sci. Eng. A*, 1998, vol. 254, pp. 76–82.
34. F.A. Mohamed and T.G. Langdon: *J. Eng. Mater. Technol.*, 1976, vol. 98 (2), pp. 125–30.
35. F.A. Mohamed and T.G. Langdon: *Metall. Trans.*, 1974, vol. 5, pp. 2339–45.
36. A. Ball and M.M. Hutchison: *Met. Sci. J.*, 1969, vol. 3, pp. 1–7.
37. J. Weertman: *J. Appl. Phys.*, 1957, vol. 28, pp. 1185–89.
38. R.L. Goetz and S.L. Semiatin: *J. Mater. Eng. Perform.*, 2001, vol. 10, pp. 710–17.
39. F.J. Humphreys and M. Hatherly: *Recrystallization and Related Annealing Phenomena*, 2nd ed., Elsevier, Amsterdam , 2004, pp. 434–41.
40. J.C. Gibeling and W.D. Nix: *Mater. Sci. Eng.*, 1980, vol. 45, pp. 123–35.
41. I.C. Hsiao and J.C. Huang: *Metall. Mater. Trans. A*, 2002, vol. 33A, pp. 1373–83.
42. K.T. Park and F.A. Mohamed: *Metall. Mater. Trans. A*, 1995, vol. 26A, pp. 3119–29.
43. D.N. Seidman, E.A. Marquis, and D.C. Dunand: *Acta Mater.*, 2002, vol. 50, pp. 4021–35.

Journal : MMTA_11661 Dispatch : 25-3-2014 Pages : 5
MS Code : 2276 ☐ LE ☐ CP ☐ TYPESET ☐ DISK